Modeling high numerical aperture optical lithography

Michael S. Yeung

Intel Corporation, MS SC1-32
2940 Mead Avenue, Santa Clara, CA 95051

ABSTRACT

Electromagnetic diffraction theory is applied to obtain a rigorous and comprehensive description of the imaging and exposure process in a projection optical system imaging a one-dimensional, periodic object in a planar layer of photoresist. The method is applicable to high numerical aperture and thick-photoresist systems, and accounts for the exposure dependent absorption characteristics of positive photoresists. It is used with the development simulator in SAMPLE to simulate the physical profile of the developed image. Theoretical and experimental results are given, which show asymmetrical variation of the developed image with focus. This asymmetry is found to depend on photoresist thickness, and the dependence is shown to be incompatible with the usual approximation of normal ray propagation in the photoresist.

1. INTRODUCTION

Most studies of the imaging process in optical lithography have been based on the scalar diffraction theory. Although such methods are believed to be adequate for systems of low numerical aperture (0.3 or less), it is not clear whether they are adequate for high numerical aperture systems. One reason is that the scalar theory does not properly take into account the effects of oblique directions of propagation of light in the latter systems. More rigorous methods, based on electromagnetic diffraction theory, would be necessary for an adequate description of such systems.

Also, most investigations of the intensity distribution within the photoresist, including a previous one by the author,[1] have employed thin-film optics methods. Such methods ignore the diffraction of light from the inhomogeneities in refractive index produced in the photoresist as a result of the photochemical reaction. A rigorous treatment of this problem would again require the use of electromagnetic theory.

In this paper, electromagnetic theory is applied to obtain a rigorous description of the combined imaging and exposure process in optical lithography for planar photoresist and thin-film layers.

In Section 2, equations for the fields incident on the entrance pupil of the optical system are given using electromagnetic diffraction theory. From these, explicit expressions for the fields arriving at the exit pupil are derived in Section 3, for an axial object. These expressions are then used in a representation of the fields incident on the photoresist surface in terms of a superposition of plane waves.

Section 4 gives a summary of a differential method for calculating the fields within the index-modulated photoresist. The discussions are restricted to one-dimensional, periodic objects. The fields so obtained are then used in Section 5 in a photoresist exposure model to describe the exposure process.

To allow comparison with experiment, the calculations are carried out through the photoresist development process, using the development simulator in SAMPLE. In Section 6, numerical results for the developed image are given. These are compared with experimental data and with the corresponding results obtained from the scalar

model of normal ray propagation in the photoresist.

2. FIELDS IN THE OBJECT SPACE

The objects dealt with in optical lithography are in the form of planar masks consisting of areas of constant transmissivity separated by essentially opague regions. In a typical projection system for lithography, the condenser optics produces an image of an extended, incoherent source on the entrance pupil of the projection lens. Consider the imaging of a point (x_0,y_0) and its neighborhood on the object plane, due to a particular point T' on the source (Fig. 1). Light from T' emerges from the condenser optics as spherical waves converging toward some point T on the entrance pupil, a distance L from the object plane. Let (x_t,y_t) be the coordinates of T on the entrance pupil. Then the distance R_t of an arbitrary point (x_1,y_1) on the object plane from T is:

$$R_t = \sqrt{(x_1-x_t)^2+(y_1-y_t)^2+L^2} = \sqrt{(\bar{x}_1-\bar{x}_t)^2+(\bar{y}_1-\bar{y}_t)^2+L^2} \tag{1}$$

where

$$\bar{x}_1 = x_1-x_0, \quad \bar{x}_t = x_t-x_0,$$
$$\bar{y}_1 = y_1-y_0, \quad \bar{y}_t = y_t-y_0 \tag{2}$$

The fields $\vec{E}_t$ and $\vec{H}_t$ incident on the object plane at (x_1,y_1) may be written as[2]:

$$\vec{E}_t = \vec{E}_t(x_1,y_1) = (\vec{t}\times\vec{E}_{t0})\times\vec{t}\,\frac{e^{-jkR_t}}{R_t} \tag{3a}$$

$$\vec{H}_t = \vec{H}_t(x_1,y_1) = \sqrt{\frac{\varepsilon_0}{\mu_0}}\,\vec{t}\times\vec{E}_t = \sqrt{\frac{\varepsilon_0}{\mu_0}}\,\vec{t}\times\vec{E}_{t0}\,\frac{e^{-jkR_t}}{R_t} \tag{3b}$$

where $k = 2\pi/\lambda$, λ being the mean wavelength in the ambient, assumed to be air, and ε_0 and μ_0 are its permittivity and permeability; $\vec{t}$ is the unit vector pointing from (x_1,y_1) to T and $\vec{E}_{t0}$ is some as yet undetermined constant vector. The above is a valid representation of a spherical wave converging toward T and obeying Maxwell's equations, provided that the distance R_t is much greater than a wavelength.[3] This is the case in optical lithography, where L may be many centimeters and $\lambda < 1$ micron.

The propagation of the fields through the object is assumed to obey the laws of geometrical optics. Thus, the object may be characterized by a function $U_0(x_1,y_1)$ such that the fields emerging from the object are given by the products of the incident fields, Eq.(3), with this function. Furthermore, $U_0(x_1,y_1)$ is assumed to be zero over the opague regions and piecewise-constant elsewhere.[4]

The above assumptions are good only if the linear dimensions of the geometric patterns comprising the object are large compared with a wavelength. In modern optical lithography, the image patterns may have linear dimensions in the micron range, and thus are not much larger than a wavelength, which may be of the order of 0.436 μm. Thus, the above assumptions may not be valid for a 1:1 projection system. On the other hand, they are valid for a reduction system having a reduction ratio of 5:1 or greater, for then an object pattern corresponding to a 1 μm image would be a factor of ten or more larger than a wavelength. Accordingly, the projection system considered here is assumed to have a reduction ratio of 5:1 or greater.[5]

The fields in the object space can now be found by applying the vector form of the Kirchoff-Huygens principle.[6] However, a straightforward application of this principle would lead to fields which do not satisfy Maxwell's equations. This is

because the discontinuities in the assumed boundary conditions on the object plane are themselves incompatible with Maxwell's equations. This difficulty can, however, be avoided by introducing fictituous line distributions of charges and currents at the boundaries of the opague regions on the object where the discontinuities occur.[7] The amended expression for the electric field $\vec{E}_2(P_2)$ at any point P_2 in the object space then becomes:

$$\vec{E}_2(P_2) = \frac{j}{4\pi\omega\varepsilon_0}\iint_{-\infty}^{\infty}\left[k^2(\vec{e}_z\times\vec{H}_t)\psi + (\vec{e}_z\times\vec{H}_t)\cdot\vec{\nabla}(\vec{\nabla}\psi) - j\omega\varepsilon_0(\vec{e}_z\times\vec{E}_t)\times\vec{\nabla}\psi\right]$$

$$\times\, U_0(x_1,y_1)\, dx_1dy_1 \qquad (4)$$

where $\psi = \exp(jkR)/R$, R being the distance between the integration point (x_1,y_1) and the field point P_2, and $\vec{e}_z$ is the unit normal to the object plane.[8]

The above expression is not restricted to small obliquity from the normal direction. However, the field point P_2 must not be too close to the object plane. When R is much greater than a wavelength, the terms involving the operator $\vec{\nabla}$, which acts on the coordinates of the integration point, can be simplified as follows:

$$\vec{\nabla}\left(\frac{e^{jkR}}{R}\right) = -\left(jk - \frac{1}{R}\right)\frac{e^{jkR}}{R}\vec{r} \approx -jk\,\frac{e^{jkR}}{R}\vec{r} \qquad (5a)$$

and similarly,

$$(\vec{e}_z\times\vec{H}_t)\cdot\vec{\nabla}\left[\vec{\nabla}\left(\frac{e^{jkR}}{R}\right)\right] \approx -k^2\left[(\vec{e}_z\times\vec{H}_t)\cdot\vec{r}\,\right]\frac{e^{jkR}}{R}\vec{r} \qquad (5b)$$

where $\vec{r}$ is the unit vector pointing from the integration point (x_1,y_1) to the field point P_2.

Eq.(4) then becomes, using Eq.(3b):

$$\vec{E}_2(P_2) = \frac{jk}{4\pi}\iint_{-\infty}^{\infty}\vec{r}\times\left\{\vec{e}_z\times\vec{E}_t - \left[\vec{r}\cdot(\vec{t}\times\vec{E}_t)\right]\vec{e}_z + (\vec{e}_z\cdot\vec{r})(\vec{t}\times\vec{E}_t)\right\} U_0(x_1,y_1)\,\frac{e^{jkR}}{R}\,dx_1dy_1 \qquad (6)$$

Suppose the point P_2 lies on the entrance pupil, with coordinates (x_2,y_2) on this plane. Then,

$$R = \sqrt{(x_1-x_2)^2+(y_1-y_2)^2+L^2} = \sqrt{(\bar{x}_1-\bar{x}_2)^2+(\bar{y}_1-\bar{y}_2)^2+L^2} \qquad (7)$$

where

$$\bar{x}_1 = x_1-x_0, \qquad \bar{x}_2 = x_2-x_0,$$
$$\bar{y}_1 = y_1-y_0, \qquad \bar{y}_2 = y_2-y_0 \qquad (8)$$

Taking into account the factor $\exp(-jkR_t)$ in Eq.(3), the argument of the phase factor $\exp(-jkR_t+jkR)$ in the integrand of Eq.(6) can be expanded as:

$$kR-kR_t = k(L_2-L_t) - k\frac{\bar{x}_2\bar{x}_1+\bar{y}_2\bar{y}_1}{L_2} + k\frac{\bar{x}_t\bar{x}_1+\bar{y}_t\bar{y}_1}{L_t} + k\frac{\bar{x}_1^2+\bar{y}_1^2}{2}\left(\frac{1}{L_2}-\frac{1}{L_t}\right)$$
$$-\left\{k\frac{(\bar{x}_1^2+\bar{y}_1^2-2\bar{x}_2\bar{x}_1-2\bar{y}_2\bar{y}_1)^2}{8L_2^3} - k\frac{(\bar{x}_1^2+\bar{y}_1^2-2\bar{x}_t\bar{x}_1-2\bar{y}_t\bar{y}_1)^2}{8L_t^3} + \ldots\right\} \qquad (9)$$

where

$$L_2 = \sqrt{L^2+\bar{x}_2^2+\bar{y}_2^2}, \qquad L_t = \sqrt{L^2+\bar{x}_t^2+\bar{y}_t^2} \tag{10}$$

The terms in braces in Eq.(9) may be neglected by applying the principle of stationary phase.[9] By this principle, the main contributions to the integral in Eq.(6) arise only from points (x_1,y_1) within a small neighborhood of (x_0,y_0), where the rate of change of phase is minimum. For such points in the neighborhood of the point of stationary phase, the terms in braces in Eq.(9) are negligible compared to 2π. This condition can be formulated as follows:

$$\frac{4\pi\bar{x}_1^2}{\lambda}\left(\frac{\bar{x}_2^2}{L_2^3}+\frac{\bar{x}_t^2}{L_t^3}\right) \ll 2\pi \tag{11}$$

We note that $\bar{x}_2/L_2$ and $\bar{x}_t/L_t$ are each of the order of the numerical aperture on the object side, which may be ≈ 0.1 for a 5:1 system. Then, for $\lambda = 0.436$ μm and $L_2 \approx$ 400 millimeters (for a 5:1 system), Eq.(11) gives:

$$\bar{x}_1 < 0.3\sqrt{\lambda L_2}/(0.2) \approx 0.6 \text{ millimeter}$$

The remaining terms in Eq.(9) may be simplified by noting that, with the help of Eq.(10):

$$k\frac{\bar{x}_1^2+\bar{y}_1^2}{2}\left(\frac{1}{L_2}-\frac{1}{L_t}\right) \approx 2\pi\,\frac{\bar{x}_1^2+\bar{y}_1^2}{4\lambda L}\left[-\frac{(\bar{x}_2^2+\bar{y}_2^2)}{L^2}+\frac{(\bar{x}_t^2+\bar{y}_t^2)}{L^2}\right]$$

This is of the same order as the terms in braces in Eq.(9), and thus may be neglected. Eq.(9) then becomes:

$$kR-kR_t = k(L_2-L_t) - \frac{2\pi}{\lambda}\left[\bar{x}_1\left(\frac{\bar{x}_2}{L_2}-\frac{\bar{x}_t}{L_t}\right)+\bar{y}_1\left(\frac{\bar{y}_2}{L_2}-\frac{\bar{y}_t}{L_t}\right)\right] \tag{12}$$

Next, insofar as only those points (x_1,y_1) on the object plane satisfying Eq.(11) contribute significantly to the image fields under consideration, the unit vector $\vec{r}$ in Eq.(6) may be replaced by a unit vector $\vec{r}_0$ pointing from (x_0,y_0) to P_2. Likewise, the unit vector $\vec{t}$ in Eqs.(6) and (3) may be replaced by a unit vector $\vec{t}_0$ pointing from (x_0,y_0) to T. The components of $\vec{r}_0$ and $\vec{t}_0$ are given by:

$$r_{0x} = \frac{\bar{x}_2}{L_2}, \qquad r_{0y} = \frac{\bar{y}_2}{L_2}, \qquad r_{0z} = \sqrt{1-r_{0x}^2-r_{0y}^2} \tag{13a}$$

$$t_{0x} = \frac{\bar{x}_t}{L_t}, \qquad t_{0y} = \frac{\bar{y}_t}{L_t}, \qquad t_{0z} = \sqrt{1-t_{0x}^2-t_{0y}^2} \tag{13b}$$

In terms of these components, Eq.(12) may be rewritten as:

$$kR-kR_t = k(L_2-L_t) - \frac{2\pi}{\lambda}\left[\bar{x}_1(r_{0x}-t_{0x})+\bar{y}_1(r_{0y}-t_{0y})\right] \tag{14}$$

For the same reason as in the replacement of $\vec{r}$ and $\vec{t}$ above, the factor $1/R_t$ in Eq.(3) and the factor $1/R$ in Eq.(6) may be replaced by $1/L_t$ and $1/L_2$, respectively.

So far, the polarization vector $\vec{E}_{t0}$ in Eq.(3) has remained arbitrary. We now require it to be normal to the unit vector $\vec{t}_0$. Then, the factor $(\vec{t}\times\vec{E}_{t0})\times\vec{t}$ in Eq.(3a), with the replacement of $\vec{t}$ by $\vec{t}_0$, becomes $\vec{E}_{t0}$.

With the above simplfications, Eq.(6) becomes, using Eqs.(3) and (14):

$$\vec{E}_2(x_2,y_2) = \frac{1}{j\lambda L_t}\, e^{-jkL_t}\, \vec{E}_{20}(r_{0x},r_{0y})\, \mathfrak{F}\{U_0;\ \frac{r_{0x}-t_{0x}}{\lambda},\frac{r_{0y}-t_{0y}}{\lambda}\}$$

$$\times\, e^{j\frac{2\pi}{\lambda}[x_0(r_{0x}-t_{0x})+y_0(r_{0y}-t_{0y})]}\, \frac{e^{jkL_2}}{L_2} \qquad (15)$$

where

$$\mathfrak{F}\{U_0;\ f_x,f_y\} = \int\int_{-\infty}^{\infty} U_0(x_1,y_1)\, e^{-2\pi j(x_1f_x+y_1f_y)}\, dx_1dy_1 \qquad (16)$$

and

$$\vec{E}_{20}(r_{0x},r_{0y}) = -\frac{1}{2}\,\vec{r}_0\times\{\vec{e}_z\times\vec{E}_{t0} - [\vec{r}_0\cdot(\vec{t}_0\times\vec{E}_{t0})]\vec{e}_z + (\vec{e}_z\cdot\vec{r}_0)(\vec{t}_0\times\vec{E}_{t0})\} \qquad (17)$$

The magnetic field $\vec{H}_2(x_2,y_2)$ is obtained from Maxwell's equations, using the fact that L_2 is much greater than a wavelength:

$$\vec{H}_2(x_2,y_2) = \sqrt{\frac{\varepsilon_0}{\mu_0}}\,\vec{r}_0\times\vec{E}_2(x_2,y_2) \qquad (18)$$

Eqs.(15) to (18) completely specify the fields incident on the entrance pupil. They are in the form of a spherical wave, $\exp(jkL_2)/L_2$, which diverges from the point (x_0,y_0) on the object plane. The polarization along the ray from (x_0,y_0) travelling in direction $\vec{r}_0$ is parallel to the vector $\vec{E}_{20}(r_{0x},r_{0y})$ given by Eq.(17), and the amplitude along this ray is proportional to the Fourier transform, Eq.(16), of the object function $U_0(x_1,y_1)$, evaluated at the spatial frequencies:

$$f_x = \frac{(r_{0x}-t_{0x})}{\lambda}, \qquad f_y = \frac{(r_{0y}-t_{0y})}{\lambda} \qquad (19)$$

3. FIELDS IN THE IMAGE SPACE

The propagation of the fields from the entrance to the exit pupil is again assumed to obey the laws of geometrical optics. From the results of the last section, through each point (x_2,y_2) on the entrance pupil passes a ray originating from the point (x_0,y_0) on the object plane, with amplitude and polarization given by Eqs.(15) to (18). In principle, this ray could be traced through the system, taking proper account of the changes in polarization at the various surfaces in the system, to find the amplitude and polarization of the fields at the corresponding point on the exit pupil. However, this would require detailed knowledge about the specific design of the system.

For the purpose of this paper, it is sufficient to consider the simple situation where the point (x_0,y_0) lies on the optical axis. In this case, each ray from this point, in the approximation of small ray aberrations, traces out a path lying entirely in one plane, the meridional plane of the ray, for a rotationally symmetrical optical system. Furthermore, provided that the angles of incidence at the

various surfaces in the system are small, the polarization vector will, to a good approximation, maintain a constant angle with the meridional plane along the entire path of the ray.[10] These approximations allow us to obtain explicit expressions for the amplitude and polarization of the fields on the exit pupil.

Let $\vec{e}_n$ be a unit vector normal to the meridional plane, in the direction of $\vec{r}_0 \times \vec{e}_z$, and $\vec{e}_p = \vec{e}_n \times \vec{r}_0$. Then $\vec{e}_p$ is a unit vector lying in the meridional plane. In terms of the components r_{0x} and r_{0y} of $\vec{r}_0$,

$$\vec{e}_n = \frac{1}{\sqrt{r_{0x}^2+r_{0y}^2}} \left[r_{0y}\vec{e}_x - r_{0x}\vec{e}_y\right] \tag{20a}$$

$$\vec{e}_p = \frac{-1}{\sqrt{r_{0x}^2+r_{0y}^2}} \left[\sqrt{1-r_{0x}^2-r_{0y}^2}\,(r_{0x}\vec{e}_x + r_{0y}\vec{e}_y) - (r_{0x}^2+r_{0y}^2)\vec{e}_z\right] \tag{20b}$$

where $\vec{e}_x$, $\vec{e}_y$ and $\vec{e}_z$ are the Cartesian unit vectors.

The polarization vector, $\vec{E}_{20}(r_{0x},r_{0y})$, of the field at the point (x_2,y_2) on the entrance pupil depends on that of the field incident on the object, $\vec{E}_{t0}$, according to Eq.(17). It is convenient to consider two orthogonal cases of incidence polarization separately:

Case I. TE polarization: $\vec{E}_{t0} \cdot \vec{e}_y = 0$.

Case II. TM polarization: $(\vec{t}_0 \times \vec{E}_{t0}) \cdot \vec{e}_y = 0$.

In the former case, the electric field of the waves incident on the object is transverse to the y-axis, while in the latter case, it is the magnetic field which is transverse. The general case of incidence polarization can be resolved into the above two orthogonal components, say, with amplitudes $\cos\chi$ and $\sin\chi$, respectively. Because the propagation equations are linear, the field on the image plane will be of the form $[\vec{E}(I)\cos\chi + \vec{E}(II)\sin\chi]$, where $\vec{E}(I)$ and $\vec{E}(II)$ are the solutions for the image field corresponding to the two orthogonal cases of incidence polarization, respectively. If the source is unpolarized, the angle χ will be uniformly distributed over the range from 0 to 2π radians. Then, the intensity distribution on the image plane, obtained by integrating the squared modulus of $[\vec{E}(I)\cos\chi + \vec{E}(II)\sin\chi]$ over χ from 0 to 2π, is clearly seen to be equal to the average of the intensity distributions corresponding to the two separate cases of polarization.

Using the fact that $\vec{E}_{t0} \cdot \vec{t}_0 = 0$, from the discussions following Eq.(14), and assuming that $\vec{E}_{t0}$ be real and of modulus R_t, so that the field incident on the object is of unit amplitude, $\vec{E}_{t0}$ can be written as:

$$\text{Case I:}\quad \vec{E}_{t0} = \frac{R_t}{\sqrt{1-t_{0y}^2}} \left[t_{0z}\vec{e}_x - t_{0x}\vec{e}_z\right] \tag{21a}$$

$$\text{Case II:}\quad \vec{E}_{t0} = \frac{R_t}{\sqrt{1-t_{0y}^2}} \left[-t_{0x}t_{0y}\vec{e}_x + (1-t_{0y}^2)\vec{e}_y - t_{0y}t_{0z}\vec{e}_z\right] \tag{21b}$$

Substituting these expressions into Eq.(17) and using Eq.(20), we obtain, after

some calculations, the following expressions for the polarization vector along the ray incident at (x_2,y_2) on the entrance pupil:

Case I polarization:

$$\vec{E}_{20}(r_{0x},r_{0y}) = R_t\left[E_{2p}(r_{0x},r_{0y})\vec{e}_p + E_{2n}(r_{0x},r_{0y})\vec{e}_n\right] \tag{22a}$$

Case II polarization:

$$\vec{E}_{20}(r_{0x},r_{0y}) = R_t\left[-E_{2n}(r_{0x},r_{0y})\vec{e}_p + E_{2p}(r_{0x},r_{0y})\vec{e}_n\right] \tag{22b}$$

where,

$$E_{2p}(r_{0x},r_{0y}) = \frac{-1}{2\sqrt{(r_{0x}^2+r_{0y}^2)(1-t_{0y}^2)}}\left\{\sqrt{1-r_{0x}^2-r_{0y}^2}\left[r_{0y}t_{0x}t_{0y} + r_{0x}(1-t_{0y}^2)\right] + r_{0x}t_{0z}\right\} \tag{23a}$$

$$E_{2n}(r_{0x},r_{0y}) = \frac{-1}{2\sqrt{(r_{0x}^2+r_{0y}^2)(1-t_{0y}^2)}}\left[r_{0x}t_{0x}t_{0y} - r_{0y}(1-t_{0y}^2) - \sqrt{1-r_{0x}^2-r_{0y}^2}\, r_{0y}t_{0z}\right] \tag{23b}$$

Let P'_2 be the point of intersection of the ray under consideration with the exit pupil, and θ and θ' be the angles that this ray makes with the optical axis in the object and image space, respectively. For an aplanatic optical system, θ and θ' are related by the Abbe sine condition:

$$\sin\theta = M \sin\theta' \tag{24}$$

where M is the magnification of the system. We assume that departure from aplanatism is small, so that Eq.(24) is obeyed to a good approximation. Then, since the ray in the image space lies, in the approximation of small ray aberrations, in a meridional plane, the unit vector $\vec{s}$ along it can be written as:

$$\vec{s} = -\sin\theta' \cos\phi\, \vec{e}_x - \sin\theta' \sin\phi\, \vec{e}_y + \cos\theta'\, \vec{e}_z \tag{25}$$

where ϕ is the angle that this meridional plane makes with the x-axis.

Using Eq.(24) and the following expressions for the components of $\vec{r}_0$ in spherical polar coordinates,

$$r_{0x} = \sin\theta\cos\phi, \quad r_{0y} = \sin\theta\sin\phi, \quad r_{0z} = \cos\theta \tag{26}$$

the components of $\vec{s}$ in Eq. (25) can be rewritten as:

$$s_x = -\frac{r_{0x}}{M}, \qquad s_y = -\frac{r_{0y}}{M}, \qquad s_z = \sqrt{1-s_x^2-s_y^2} \tag{27}$$

The electric field at P'_2 must be perpendicular to $\vec{s}$ and, according to the above discussions, makes the same angle with the meridional plane as $\vec{E}_{20}(r_{0x},r_{0y})$. Let $\vec{E}'_{20}(s_x,s_y)$ be a vector at P'_2 in the direction of the electric field and having the same magnitude as $\vec{E}_{20}(r_{0x},r_{0y})$. Then the components of these two vectors normal or parallel to the meridional plane must be of equal magnitude. The perpendicular component of $\vec{E}'_{20}$ still lies in the direction of $\vec{e}_n$, given by Eq.(20a), but the parallel component of $\vec{E}'_{20}$ now lies in the direction of a unit vector $\vec{e}'_p = \vec{e}_n \times \vec{s}$:

$$\vec{e}'_p = \frac{1}{\sqrt{s_x^2+s_y^2}}\left[\sqrt{1-s_x^2-s_y^2}\,(s_x\vec{e}_x + s_y\vec{e}_y) - (s_x^2+s_y^2)\vec{e}_z\right] \tag{28}$$

Thus, the polarization vector along the ray in the image space through P'_2 is:

Case I polarization:

$$\vec{E}'_{20}(s_x,s_y) = R_t\left[E_{2p}(r_{0x},r_{0y})\vec{e}'_p + E_{2n}(r_{0x},r_{0y})\vec{e}_n\right] \tag{29a}$$

Case II polarization:

$$\vec{E}'_{20}(s_x,s_y) = R_t\left[-E_{2n}(r_{0x},r_{0y})\vec{e}'_p + E_{2p}(r_{0x},r_{0y})\vec{e}_n\right] \tag{29b}$$

where $E_{2n}(r_{0x},r_{0y})$ and $E_{2p}(r_{0x},r_{0y})$ are still given by Eq.(23).

Using the fact that the field incident on the entrance pupil, given by Eq.(15), is in the form of a spherical wave diverging from the point (x_0,y_0) on the object plane, the field on the exit pupil is, in the approximation of geometrical-optics propagation through the projection lens, also in the form of a spherical wave. The latter converges toward the Gaussian image point P^*_0 and has the following representation[11]:

$$\vec{E}'(P'_2) = A(s_x,s_y)\,\frac{\vec{E}'_{20}(s_x,s_y)}{R_t}\,\frac{e^{jk[\Phi(s_x,s_y)-r']}}{r'} \tag{30}$$

where r' is the distance of the point P'_2 on the exit pupil from the Gaussian image point, $\Phi(s_x,s_y)$ the aberration function regarded as a function of the direction cosines s_x and s_y of the ray through P'_2, and $A(s_x,s_y)$ a complex amplitude factor still to be determined.

The amplitude factor $A(s_x,s_y)$ can be found by using the intensity law of geometrical optics. For this purpose, it is again sufficient to ignore ray aberrations and regard the ray through P'_2 as being directed exactly toward the Gaussian image point and obeying the Abbe sine condition.

Consider the cone of rays in the object space originating from the axial point $(x_0,y_0) = (0,0)$ on the object plane and lying within an element of solid angle $\sin\theta\, d\theta d\phi$. In the image space, these rays converge toward the axial image point P^*_0 and lie within the element of solid angle $\sin\theta'\, d\theta' d\phi$, where θ' is related to θ by Eq.(24). Applying the intensity law to these two cones of rays, using Eqs.(15) and (30) for the fields on the entrance and exit pupils, respectively, and ignoring energy losses within the system, we obtain:

$$|A(s_x,s_y)|^2\,\frac{|\vec{E}'_{20}(s_x,s_y)|^2}{R_t^2}\,\sin\theta'\,d\theta' d\phi = \frac{1}{(\lambda L_t)^2}|\vec{E}_{20}(r_{0x},r_{0y})|^2 \times |\mathfrak{F}\{U_0;\frac{r_{0x}-t_{0x}}{\lambda},\frac{r_{0y}-t_{0y}}{\lambda}\}|^2\,\sin\theta\,d\theta d\phi$$

Since R_t is practically equal to L_t, according to the discussions following Eq.(14), and $|\vec{E}'_{20}| = |\vec{E}_{20}|$, the above equation gives for $A(s_x,s_y)$:

$$A(s_x,s_y) = \frac{M}{\lambda}\sqrt{\frac{\cos\theta'}{\cos\theta}}\,\mathfrak{F}\{U_0;\frac{r_{0x}-t_{0x}}{\lambda},\frac{r_{0y}-t_{0y}}{\lambda}\} \tag{31}$$

where we have omitted an unimportant phase factor and used the fact that $\cos\theta\, d\theta = M \cos\theta'\, d\theta'$.

Let the actual image plane be displaced with respect to the Gaussian image plane, in the negative z-direction, by an amount Δ.[12] Then the electric field $\vec{E}_i(x,y)$ at a point (x,y) on the image plane is given by[13]:

$$\vec{E}_i(x,y) = \frac{1}{j\lambda}\iint_{\Omega} A(s_x,s_y)\,\frac{\vec{E}'_{20}(s_x,s_y)}{R_t}\,\frac{e^{jk[\Phi(s_x,s_y)-s_z\Delta+s_xx+s_yy]}}{s_z}\,ds_x ds_y \tag{32}$$

where the integral is taken over the solid angle Ω subtended by the exit pupil at the Gaussian image point.

Without loss of generality, the image plane can be chosen to be the outer surface of the resist. Then Eq.(32) has the simple physical interpretation that the field incident on the resist surface, $\vec{E}_i(x,y)$, consists of a superposition of infinite plane waves, $\exp[jk(s_xx+s_yy)]$, propagating in directions $\vec{s}$. The electric field amplitude of the plane wave with direction cosines s_x and s_y is $\vec{B}(s_x,s_y)$, where:

$$\vec{B}(s_x,s_y) = \frac{1}{j\lambda}\,A(s_x,s_y)\,\frac{\vec{E}'_{20}(s_x,s_y)}{R_t}\,\frac{e^{jk[\Phi(s_x,s_y)-s_z\Delta]}}{s_z}\,ds_x ds_y \tag{33}$$

The corresponding amplitude of the magnetic field is $\sqrt{(\varepsilon_0/\mu_0)}\;\vec{s}\times\vec{B}(s_x,s_y)$.

The propagation of each such plane wave through the resist and underlying thin films can be considered separately. The total field within the resist, due to the particular source point T' in one of the two modes of polarization given by Eq.(29), is then obtained by superposing the individual fields due to these plane waves.

4. FIELDS IN THE RESIST

The photochemical reaction occurring in the resist during exposure causes the resist absorption coefficient to decrease, an effect commonly referred to as bleaching. For simplicity, we limit our treatment of this effect to one-dimensional, periodic objects. Thus, the object function $U_0(x_1)$ is independent of y_1 and periodic in x_1, with a period D. Also, the substrate is assumed to be composed of planar, homogeneous layers and the resist to be uniform in thickness and initially homogeneous. Then, due to bleaching, a one-dimensional periodic modulation in the dielectric constant of the resist is produced, causing the resist to act like a diffraction grating. The resist dielectric constant can then be represented by a function $\varepsilon(x,z)$, independent of y and periodic in x with period $d = MD$. Here, the coordinate z is measured inwards from the outer surface of the resist, where $z = 0$.

The propagation of an incident plane wave, $\vec{B}(s_x,s_y)\exp[jk(s_xx+s_yy)]$, through such a resist layer can be rigorously described using the electromagnetic theory of diffraction gratings.[14] Because the direction cosines s_x and s_y may take on arbitrary values satisfying:

$$\sqrt{s_x^2+s_y^2} \leq NA \tag{34}$$

where NA is the numerical aperture of the system, the incident wave vector $\vec{s}$ is, in general, not perpendicular to the grating 'grooves' along the y-direction. Hence, it is necessary to employ a formalism applicable to diffraction gratings in this general configuration, referred to as the conical diffraction mounting.

The formalism which is simplest to implement numerically is the differential method.[15] In this method, the Cartesian field components at a point (x,y,z) within the resist are expanded in terms of elementary, pseudo-periodic functions $\exp(jks_{xn}x)$:

$$E_x(x,y,z) = e^{jks_y y} \sum_n E_{xn}(z)\, e^{jks_{xn}x} \tag{35}$$

where

$$s_{xn} = s_x + \frac{n\lambda}{d} \tag{36}$$

Similar expansions are introduced for $E_y(x,y,z)$, $E_z(x,y,z)$, $H_x(x,y,z)$, $H_y(x,y,z)$ and $H_z(x,y,z)$. These expansions are possible because, by the periodicity of the dielectric constant in x, together with the spatial dependence, $\exp[jk(s_x x+s_y y)]$, of the incident wave, each component of the electric or magnetic field must satisfy the pseudo-periodicity condition:

$$E_x(x+d,y+\delta,z) = e^{jks_x d}\, e^{jks_y \delta}\, E_x(x,y,z) \tag{37}$$

where δ is an arbitrary displacement in the y-direction. Similar conditions hold for the other field components.

Substituting the above expansions for the field components in Maxwell's equations, the following system of differential equations can be derived[16]:

$$\frac{dE_{xn}(z)}{dz} = jks_{xn}E_{zn}(z) + j\omega\mu_0 H_{yn}(z) \tag{38a}$$

$$\frac{dE_{yn}(z)}{dz} = jks_y E_{zn}(z) - j\omega\mu_0 H_{xn}(z) \tag{38b}$$

$$\frac{dH_{xn}(z)}{dz} = jks_{xn}H_{zn}(z) - j\omega\varepsilon_0 \sum_m \varepsilon_{n-m}(z)E_{ym}(z) \tag{38c}$$

$$\frac{dH_{yn}(z)}{dz} = jks_y H_{zn}(z) + j\omega\varepsilon_0 \sum_m \varepsilon_{n-m}(z)E_{xm}(z) \tag{38d}$$

where

$$E_{zn}(z) = \frac{k}{\omega\varepsilon_0} \sum_m \left[\frac{1}{\varepsilon}\right]_{n-m}(z) \left[s_y H_{xm}(z) - s_{xm}H_{ym}(z)\right] \tag{39a}$$

and

$$H_{zn}(z) = \frac{-k}{\omega\mu_0} \left[s_y E_{xn}(z) - s_{xn}E_{yn}(z)\right] \tag{39b}$$

In the above equations, $\varepsilon_{n-m}(z)$ is the (n-m)th Fourier coefficient in the Fourier-series expansion of the dielectric constant $\varepsilon(x,z)$ for fixed z, and $(1/\varepsilon)_{n-m}(z)$ that for $[1/\varepsilon(x,z)]$.

In practice, the infinite sums in Eqs.(35), (38) and (39a) are truncated to a finite number, N, of terms. Then, by substituting Eq.(39) into Eq.(38), a system of coupled differential equations in the 4N unknown functions $E_{xn}(z)$, $E_{yn}(z)$, $H_{xn}(z)$ and $H_{yn}(z)$ is obtained. To set up the necessary boundary conditions for this problem, we introduce Rayleigh expansions for the fields in the air and substrate regions.

Let z_s be the distance between the outer resist surface and the interface between the substrate and the innermost thin-film layer. Then the fields in the air, $z \leq 0$, and substrate, $z \geq z_s$, have expansions similar to Eq.(35), but with known forms for the functions $E_{\mu n}(z)$ and $H_{\mu n}(z)$, where μ stands for x, y or z. For the y-components, these are:

For $z \leq 0$:

$$E_{yn}(z) = A_{1n}\, e^{j\beta_{1n}z} + B_{1n}\, e^{-j\beta_{1n}z}, \qquad H_{yn}(z) = P_{1n}\, e^{j\beta_{1n}z} + Q_{1n}\, e^{-j\beta_{1n}z} \tag{40}$$

For $z \geq z_s$:

$$E_{yn}(z) = A_{2n}\, e^{j\beta_{2n}z}, \qquad H_{yn}(z) = P_{2n}\, e^{j\beta_{2n}z} \tag{41}$$

where

$$\beta_{1n} = k\sqrt{1-s_y^2-s_{xn}^2}, \qquad \beta_{2n} = k\sqrt{\varepsilon_{r2}-s_y^2-s_{xn}^2} \tag{42}$$

ε_{r2} being the dielectric constant of the substrate. The x-components are then given by:

For $z \leq 0$:

$$E_{xn}(z) = \frac{1}{k^2(1-s_y^2)}\left[\omega\mu_0\beta_{1n}(P_{1n}e^{j\beta_{1n}z} - Q_{1n}e^{-j\beta_{1n}z}) - k^2 s_y s_{xn} E_{yn}(z)\right] \tag{43a}$$

$$H_{xn}(z) = \frac{-1}{k^2(1-s_y^2)}\left[\omega\varepsilon_0\beta_{1n}(A_{1n}e^{j\beta_{1n}z} - B_{1n}e^{-j\beta_{1n}z}) + k^2 s_y s_{xn} H_{yn}(z)\right] \tag{43b}$$

For $z \geq z_s$:

$$E_{xn}(z) = \frac{1}{k^2(\varepsilon_{r2}-s_y^2)}\left(\omega\mu_0\beta_{2n}P_{2n} - k^2 s_y s_{xn} A_{2n}\right) e^{j\beta_{2n}z} \tag{44a}$$

$$H_{xn}(z) = \frac{-1}{k^2(\varepsilon_{r2}-s_y^2)}\left(\omega\varepsilon_{r2}\varepsilon_0\beta_{2n}A_{2n} + k^2 s_y s_{xn} P_{2n}\right) e^{j\beta_{2n}z} \tag{44b}$$

Eq.(41) incorporates the boundary condition that there be no incoming wave in the substrate region. The other boundary condition states that there is only one incoming wave, namely, that corresponding to $n = 0$, in the air region. Hence, the coefficients A_{1n} and P_{1n} in Eq.(40) all vanish except for $n = 0$, in which case they are equal to the y-components of $\vec{B}(s_x, s_y)$ and $\sqrt{(\varepsilon_0/\mu_0)}\,\vec{s}\times\vec{B}(s_x, s_y)$, respectively.

Because the diffracted wave amplitudes B_{1n} and Q_{1n} are unknown to begin with, it is not possible to set up the correct initial values for $E_{xn}(0)$, $E_{yn}(0)$, $H_{xn}(0)$ and $H_{yn}(0)$ at $z = 0$ to start the numerical integration of Eq.(38). Instead, in one method of solution, the shooting method, one starts with arbitrary values of the coefficients A_{2n} and P_{2n} and constructs the initial values $E_{xn}(z_s)$, $E_{yn}(z_s)$, $H_{xn}(z_s)$ and $H_{yn}(z_s)$ at $z = z_s$ using Eqs.(41) and (44). Eq.(38) is then integrated backwards

numerically up to z = 0.[17] By means of Eqs.(40) and (43), a set of coefficients A_{1n} and P_{1n} is obtained from the resulting values of $E_{xn}(0)$, $E_{yn}(0)$, $H_{xn}(0)$ and $H_{yn}(0)$.

Let $\vec{\psi}_1$ be the column vector, with 2N elements, obtained by juxtaposing the coefficients A_{1n} and P_{1n}, and $\vec{\psi}_2$ be similiarly defined for A_{2n} and P_{2n}. In general, the vector $\vec{\psi}_1$ obtained in the above way, for an arbitrary choice of $\vec{\psi}_2$, is different from the one corresponding to the given incident wave. However, by the linearity of the equations involved, $\vec{\psi}_1$ must be linearly related to $\vec{\psi}_2$:

$$\vec{\psi}_1 = \underset{\sim}{W}\, \vec{\psi}_2 \tag{45}$$

where $\underset{\sim}{W}$ is a 2N×2N matrix. By starting with 2N linearly independent initial vectors $\vec{\psi}_2$ and obtaining the 2N corresponding vectors $\vec{\psi}_1$ in the above way, the matrix $\underset{\sim}{W}$ is completely determined. Then, Eq.(45) is inverted, using the vector $\vec{\psi}_1$ corresponding to the given incident wave, to obtain the correct initial vector $\vec{\psi}_2 = \underset{\sim}{W}^{-1}\, \vec{\psi}_1$. The corresponding initial values $E_{xn}(z_s)$, $E_{yn}(z_s)$, $H_{xn}(z_s)$ and $H_{yn}(z_s)$ are obtained from Eqs.(41) and (44). Eq.(38) is then integrated backwards once more to determine the values of $E_{xn}(z)$, $E_{yn}(z)$, $H_{xn}(z)$ and $H_{yn}(z)$ at chosen values of z within the resist. The corresponding values of $E_{zn}(z)$ are obtained from Eq.(39a). Then, by means of Eq.(35) and similar expressions for $E_y(x,y,z)$ and $E_z(x,y,z)$, the electric field $\vec{E}(x,y,z)$ within the resist is found.

The total field within the resist is obtained by superposing the fields $\vec{E}(x,y,z)$ found in the above manner, for the various plane waves $\vec{B}(s_x,s_y)\exp[jk(s_x x+s_y y)]$ contained the incident field $\vec{E}_i(x,y)$. The squared modulus, I(x,z), of the total field is a function only of x and z, for the one-dimensional objects considered here.

For an unpolarized source, the above calculations must be repeated for the two orthogonal cases of incidence polarization given by Eq.(29) and the average I(x,z) taken. Furthermore, for an extended, incoherent source, the calculations must be repeated for each point T' into which the source is subdivided. The final, average I(x,z) obtained in this way is then used below to describe the exposure of the resist.

5. PHOTORESIST PROCESS MODEL

In this section the Dill model of positive photoresist[18] is used to describe the exposure process. Here, the absorption coefficient of the resist is governed by the molar concentration of a single species of photoactive compound, known as the inhibitor. Let M(x,z,t) represent the concentration of inhibitor within the resist, at time t, normalized to the unexposed, uniform concentration at t = 0. Then the complex refractive index of the resist, n(x,z,t), is given by:

$$n(x,z,t) = n_0 + \frac{j\lambda}{4\pi}\,[A\,M(x,z,t) + B] \tag{46}$$

where n_0, A and B are positive constants characterizing the resist. From this expression, it can be seen that (A+B) and B are the absorption coefficients of the unexposed (M = 1) and fully exposed (M = 0) resist, respectively.

The photochemical reaction occuring during exposure converts the inhibitor into reaction products, resulting in a decrease in the absorption coefficient of the resist. Let P(x,z,t) be the average local rate of energy dissipation per unit volume in the resist. Then, according to the Dill model[19]:

$$\frac{\partial M(x,z,t)}{\partial t} = \frac{-P(x,z,t)}{A\,M(x,z,t) + B}\,M(x,z,t)\,C \tag{47}$$

where C is a constant characterizing the optical sensitivity of the resist. By Poynting's theorem, P(x,z,t) is related to the local electric field $\vec{E}_r(x,z,t)$ by:

$$P(x,z,t) = n_0 \frac{\lambda}{4\pi}\,[A\,M(x,z,t) + B]\,\varepsilon_0\omega\,|\vec{E}_r(x,z,t)|^2 \tag{48}$$

Thus, Eq.(47) becomes

$$\frac{\partial M(x,z,t)}{\partial t} = -\frac{\lambda}{4\pi}\,n_0\varepsilon_0\omega\,|\vec{E}_r(x,z,t)|^2\,M(x,z,t)\,C \tag{49}$$

Since the electric field $\vec{E}_r(x,z,t)$ is dependent on the refractive index of the resist, and thus on M(x,z,t) through Eq.(46), Eq.(49) is a non-linear differential equation for M(x,z,t). For numerical integration, the equation is discretized in t, using a sufficiently small time increment Δt to achieve convergence of the results. At the beginning of the nth time step, t_n, n = 1,2,..., the refractive index $n(x,z,t_n)$ is calculated using the inhibitor distribution $M(x,z,t_{n-1})$ obtained at the end of the previous time step, with $M(x,z,t_0) = 1$. The dielectric constant $\varepsilon(x,z)$ is set equal to $n^2(x,z,t_n)$ and the average squared modulus, I(x,z), of the electric field within the resist then calculated using the method discussed in the last section. The inhibitor distribution is then changed according to:

$$M(x,z,t_n) = M(x,z,t_{n-1})\,e^{-\frac{\lambda}{4\pi}\,n_0\varepsilon_0\omega\,I(x,z)\,C\,\Delta t} \tag{50}$$

The above calculations are repeated for successive time steps t_{n+1}, ..., until the desired total exposure dose is delivered through the optical system. The final inhibitor concentration so obtained, M(x,z,τ), where τ is the exposure time, can then be used in a development model to simulate the physical profile of the developed image.

The development model used here is the one contained in the general lithography simulator SAMPLE.[20] Here, the dissolution of the resist in the developer is assumed to be a surface-rate limited process. The dissolution rate R(x,z) is determined by the local value of M(x,z,τ) according to the following empirical relation[21]:

$$R(x,z) = \frac{1}{\left[\frac{1}{R_1}\{1 - M(x,z,\tau)\,e^{-R_3[1-M(x,z,\tau)]}\} + \frac{1}{R_2}\,M(x,z,\tau)\,e^{-R_3[1-M(x,z,\tau)]}\right]} \tag{51}$$

where R_1, R_2 and R_3 are parameters characterizing the resist-developer combination.

SAMPLE also provides for simulating the effects of post-exposure baking, a pre-development step sometimes used in processing to smooth out the standing-wave pattern in the developed resist profile. This is accomplished by convoluting the inhibitor distribution M(x,z,τ) with a Gaussian function, with a suitable choice of the diffusion length, σ, before using it in Eq.(51). The simulator then generates the two-dimensional physical profile of the image for a given develop time.

6. APPLICATIONS

An important issue in high numerical aperture optical lithography is the ability to control the critical dimension (CD) of a developed feature under a given set of

processing conditions.[22] Such information can conveniently be obtained from a plot of the CD against the defocus distance, for different values of the exposure dose.

Fig. 2 gives examples of CD versus focus plots calculated by the vector method described above, for two different thicknesses of the photoresist. The modeling parameters are given in Table 1. This figure can be compared with corresponding experimental data given in Fig. 3. In both figures, the variation of CD is seen to be asymmetrical with respect to focus. Furthermore, in both figures, the asymmetry is seen to be more pronounced for the thicker photoresist. On the other hand, calculations based on the customary, scalar model of normal ray propagation in the photoresist, in the case of no aberrations in the optical system, would predict a symmetrical variation of CD with focus, for any given thickness of the photoresist. This is shown in Fig. 4, which gives the corresponding plots obtained from the scalar model.

Asymmetry of the developed image with respect to focus can also be caused by aberrations in the optical system. For the axial, grating object under consideration, the only primary aberration that can impart asymmetry to the aerial image with respect to focus is spherical aberration. However, the scalar model, which assumes normal ray propagation in the photoresist, would predict that the asymmetry in the resulting CD versus focus plot should, to first approximation, be independent of photoresist thickness. This is illustrated in Fig. 5, which gives the results of calculations based on the scalar model, for a system possessing an assumed amount of third-order spherical aberration equivalent to a maximum value of $\Phi(s_x, s_y)$ of about one-fifth of a wavelength. Here, the plots for the two different photoresist thicknesses, although they are both asymmetrical due to the aberration, are very similar in appearance. This is inconsistent with the experimental data given in Fig. 3, which show a significantly greater asymmetry in the case of the thicker photoresist. On the other hand, the results given by the vector method, as shown in Fig. 2, indicate a change in the asymmetry in going to the thicker photoresist of about the same amount as the data, without introducing artificial aberrations.

The physical profile of the developed image, besides the CD, is also of interest in lithography. Fig. 6 gives a through focus sequence of SEM pictures of developed photoresist images, together with the simulation results obtained by the vector method. The SEM pictures show that the photoresist profile behaves qualitatively differently on either side of the best focus. When the Gaussian image plane is moved in the direction toward the projection lens, the photoresist sidewalls tend to remain straight, although they are gradually tilted away from the vertical. In the opposite direction of defocus, however, the profile tends to become dome-shaped. This behavior is in qualitative agreement with the simulation results given in the same figure.

7. CONCLUSIONS

We have described a method, based upon electromagnetic diffraction theory, for calculating the electric field within a planar photoresist layer in an optical lithography system. The method is applicable to high numerical aperture and thick-photoresist systems, and takes into account diffraction of light due to bleaching of the photoresist. By combining it with the development simulator in SAMPLE, we have obtained numerical results showing asymmetrical variation of the developed image with focus. The predicted dependence of this asymmetry on photoresist thickness has been observed experimentally. Finally, we have shown that this dependence is incompatible with the scalar model of normal ray propagation in the photoresist, even when aberrations in the optical system are taken into account.

8. ACKNOWLEDGEMENTS

The author wishes to thank Paul Chien, Ling Liauw and Michelle Sugasawara for their electrical CD data, and Vahid Eshraghi and Jeff Lewis for their SEM pictures.

9. REFERENCES

1. M. Yeung, "Modeling Aerial Images in Two and Three Dimensions", Proc. Kodak Microelectronics Seminar INTERFACE '85, 115 (1986).
2. Assuming a time dependence of exp(-jωt), ω being the mean angular frequency of the light.
3. J. Stratton, "Electromagnetic Theory" (McGraw-Hill, New York, 1941), p.393.
4. Discontinuities in $U_0(x_1,y_1)$ are assumed to occur only at the boundaries of the opague areas but not in the regions of constant transmissivity.
5. For a 1:1 projection system, the fields emerging from the object would have to be found by rigorously solving the problem of diffraction of the incident waves at the boundaries of the object.
6. J. Stratton, ibid., Sec. 8.14.
7. S. Silver, "Microwave Antenna Theory and Design" (Peter Peregrinus Ltd., London, UK, 1986), Sec. 5.8, or J. Stratton, ibid., Sec. 8.15.
8. S. Silver, ibid, p.160.
9. M. Born and E. Wolf, "Principles of Optics" (Pergamon Press, New York, 1975), p.386.
10. R. Richards and E. Wolf, "Electromagnetic Diffraction in Optical Systems II. Structure of the Image Field in an Aplanatic System", Proc. Roy. Soc. A 253, 358 (1959).
11. E. Wolf, "Electromagnetic Diffraction in Optical Systems I. An Integral Representation of the Image Field", Proc. Roy. Soc. A 253, 349 (1959).
12. The sign of Δ is chosen to agree with the focus convention used for the experimental data discussed in Section 6. In the usual lithography situation, Δ is of the order of the depth of focus of the system. For such small values of defocus, the argument of the principle of stationary phase used in Section 2, leading to the omission of the high-order terms in Eq.(9), is expected to remain valid.
13. E. Wolf, ibid.
14. R. Petit, Ed. "Electromagnetic Theory of Gratings" (Springer-Verlag, New York, 1980).
15. P. Vincent et al., "Computation of the Efficiencies and Polarization Effects of XUV Gratings used in Classical and Conical Mountings", Nucl. Instr. Meth. 152, 123 (1978).
16. R. Petit, ibid., Chap. 4.
17. Where one or more thin-film layers are present, the fields at the inner surface of the resist are first calculated by the methods of thin-film optics.
18. F. Dill et al., "Characterization of Positive Photoresist", IEEE Trans. Electron Devices ED-22, 445 (1975).
19. F. Dill et al., "Modeling Projection Printing of Positive Photoresists", IEEE Trans. Electron Devices ED-22, 456 (1975).
20. W. Oldham et al., "A General Simulator for VLSI Lithography and Etching Processes: Part I - Application to Projection Lithography", IEEE Trans. Electron Devices ED-26, 717 (1979).
21. D. Kim et al., "Characterization and Modeling of a Resist with Built-in Induction Effect", Proc. Kodak Microelectronics Seminar INTERFACE '83, 112 (1984).
22. In this section, CD is defined to be the width of the developed resist profile, measured at the 'waist' of the standing-wave pattern nearest the substrate.

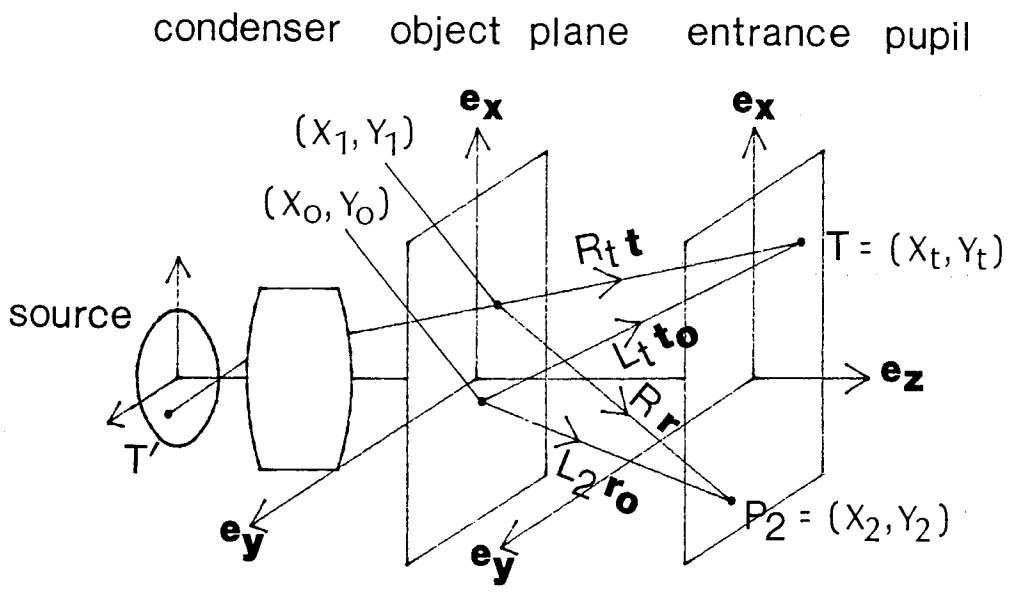

Figure 1. Rays in the object space used to describe the imaging due to a source point T'.

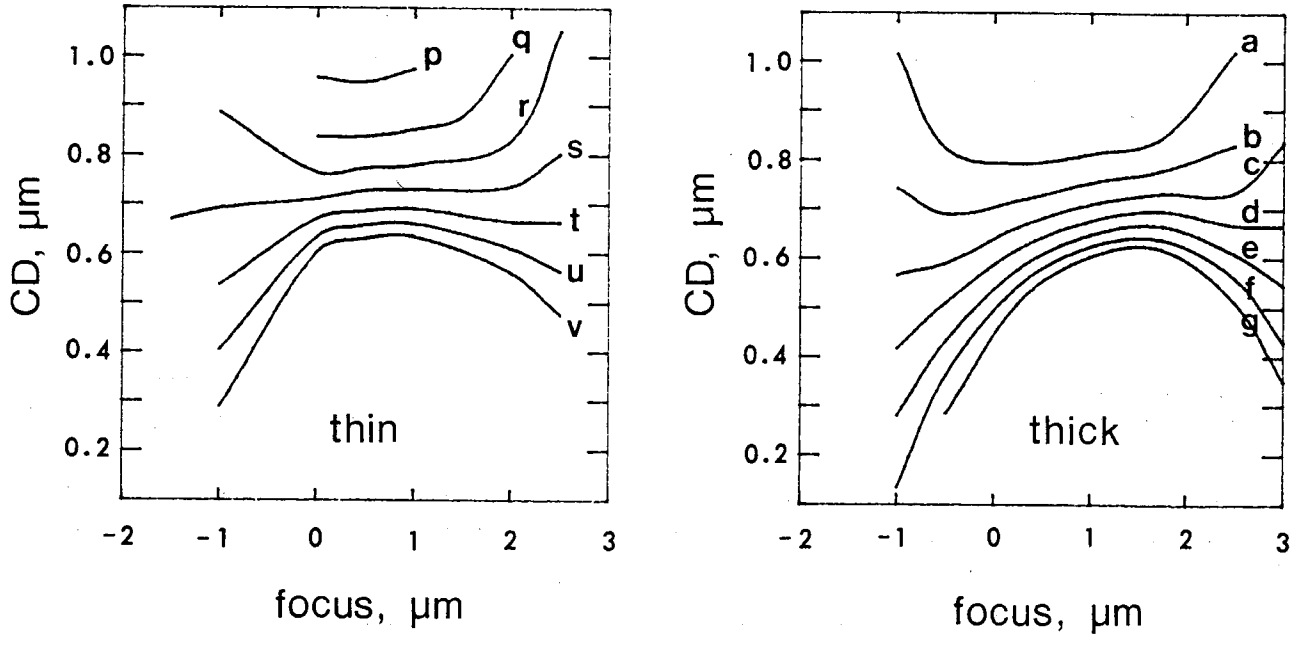

Figure 2. Calculated CD versus focus plots based on the vector method, for a one-dimensional, grating object consisting of equal lines and spaces of width 0.80 µm. The optical system was a 5:1 reduction system with NA = 0.42, λ = 0.4358 µm and condenser NA to lens NA ratio = 0.5. The photoresist thicknesses (AZ1312 and AZ1318) for the left (thin) and right (thick) plots were 1.24 and 2.10 µm, resp. The substrate was the same in both cases, and consisted of silicide, polysilicon and oxide films over silicon. The curves, labelled (p) to (v) and (a) to (g) in the left and right plots, resp., correspond to different values of the exposure dose. In terms of the threshold dose, that is, the minimum dose required to develop out a large, clear region, these are:

Left: (p) 1.11, (q) 1.29, (r) 1.48, (s) 1.66, (t) 1.85, (u) 2.03, and (v) 2.22.
Right: (a) 1.28, (b) 1.47, (c) 1.67, (d) 1.86, (e) 2.06, (f) 2.26, and (g) 2.45.

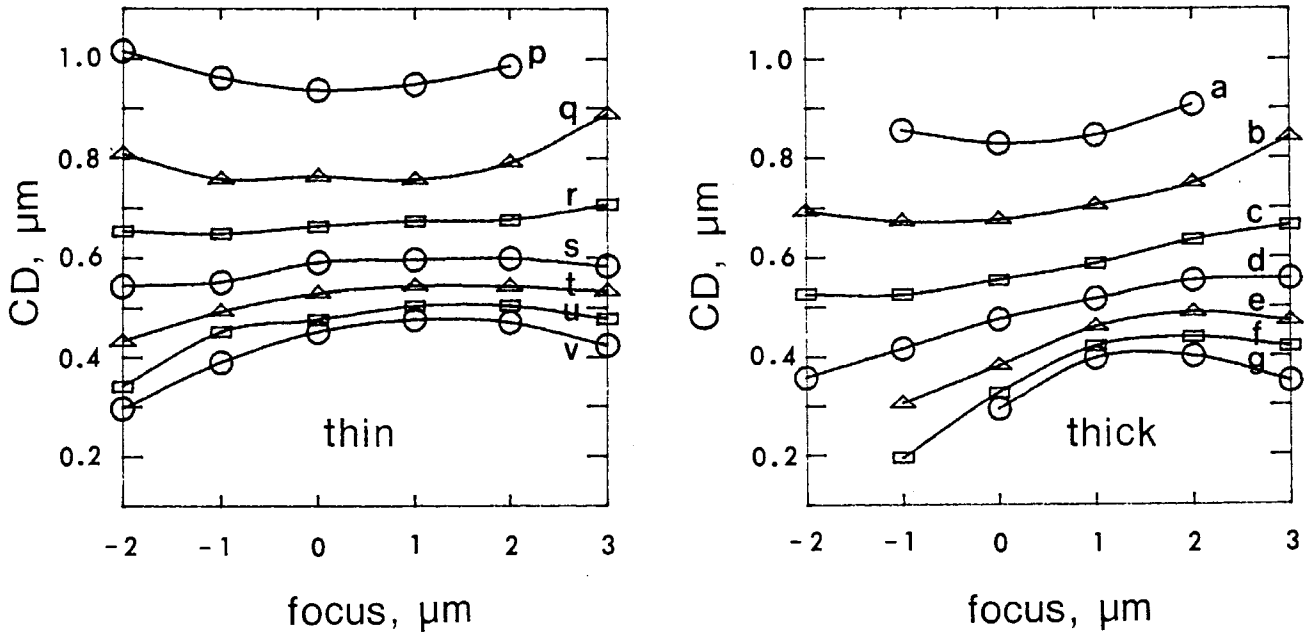

Figure 3. Experimental CD versus focus plots, obtained by electrical measurement of anisotropically etched silicide-polysilicon lines. The experimental conditions were the same as the modeling parameters given in the caption of Fig. 2.

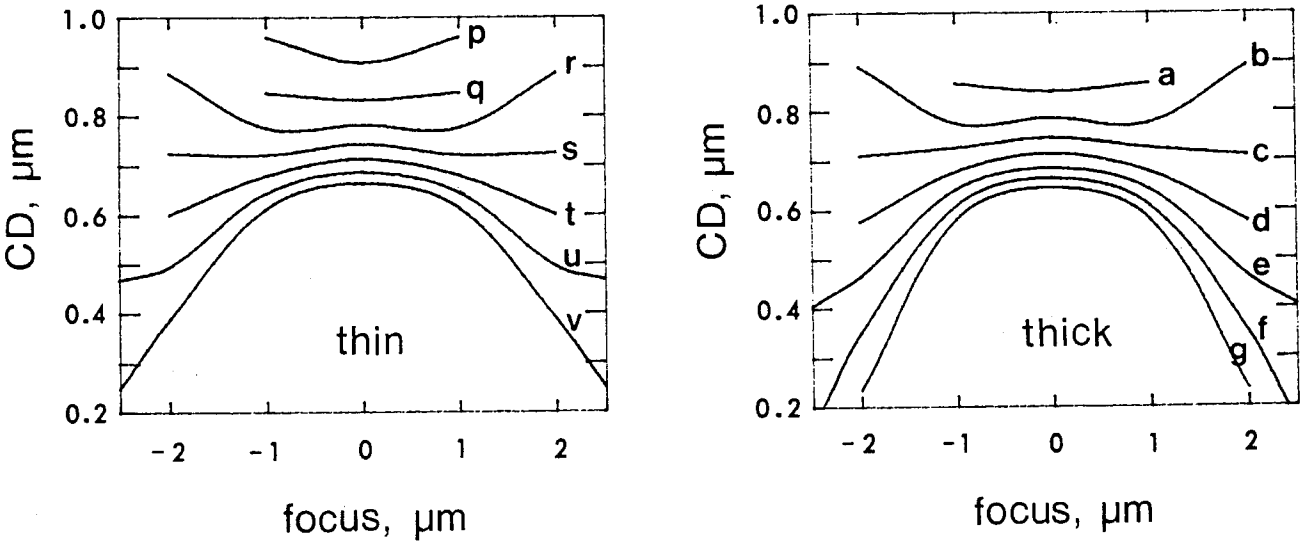

Figure 4. Calculated CD versus focus plots based on the scalar model of normal ray propagation in the photoresist, assuming no aberrations in the optical system. The modeling parameters are the same as those of Fig. 2.

Table 1. Photoresist Modeling Parameters

Exposure parameter	Value	Development parameter	Value
A	0.54 μm^{-1}	R_1	0.18 $\mu m\ s^{-1}$
B	0.20 μm^{-1}	R_2	0.00005 $\mu m\ s^{-1}$
C	0.010 $cm^2\ mJ^{-1}$	R_3	6.4
σ	0.04 μm	Develop time	60 s

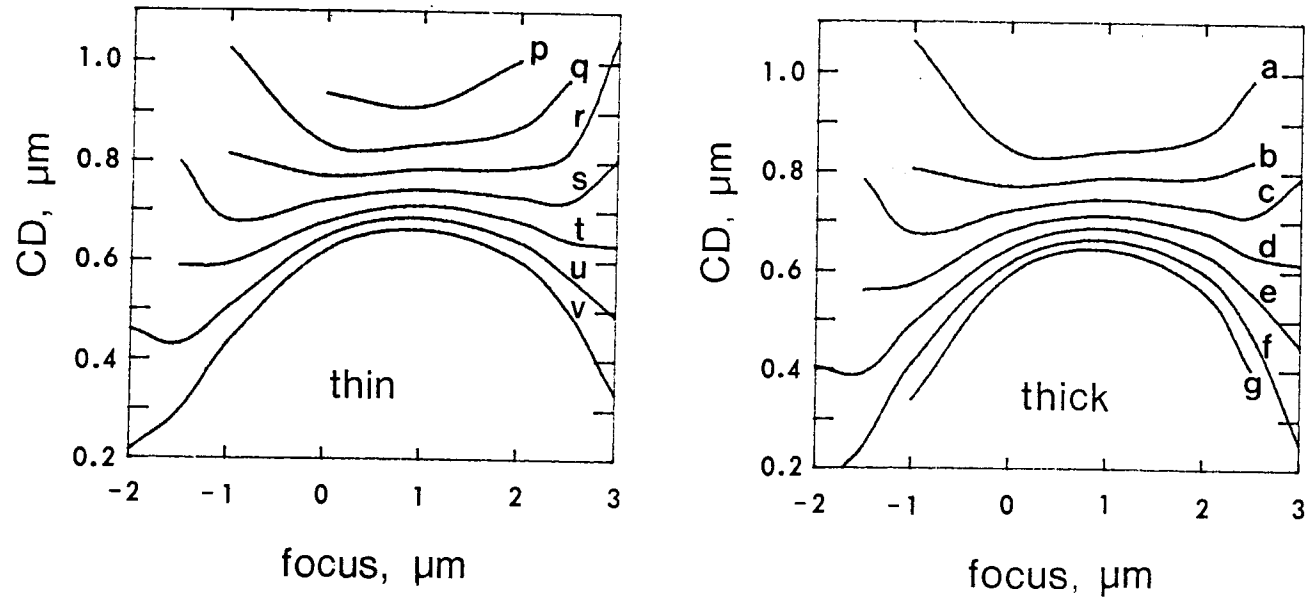

Figure 5. Calculated CD versus focus plots based on the scalar model of normal ray propagation in the photoresist, assuming the presence of third-order spherical aberration in the optical system, described by an amount of longitudinal spherical aberration equal to 2.0 µm. This means that the marginal rays come to a focus 2.0 µm closer to the lens than the paraxial rays. For NA = 0.42 and λ = 0.4358 µm, this is equivalent to a maximum value of the aberration function $\Phi(s_x,s_y)$ of about $\lambda/5$. The other modeling parameters are the same as those of Fig. 2.

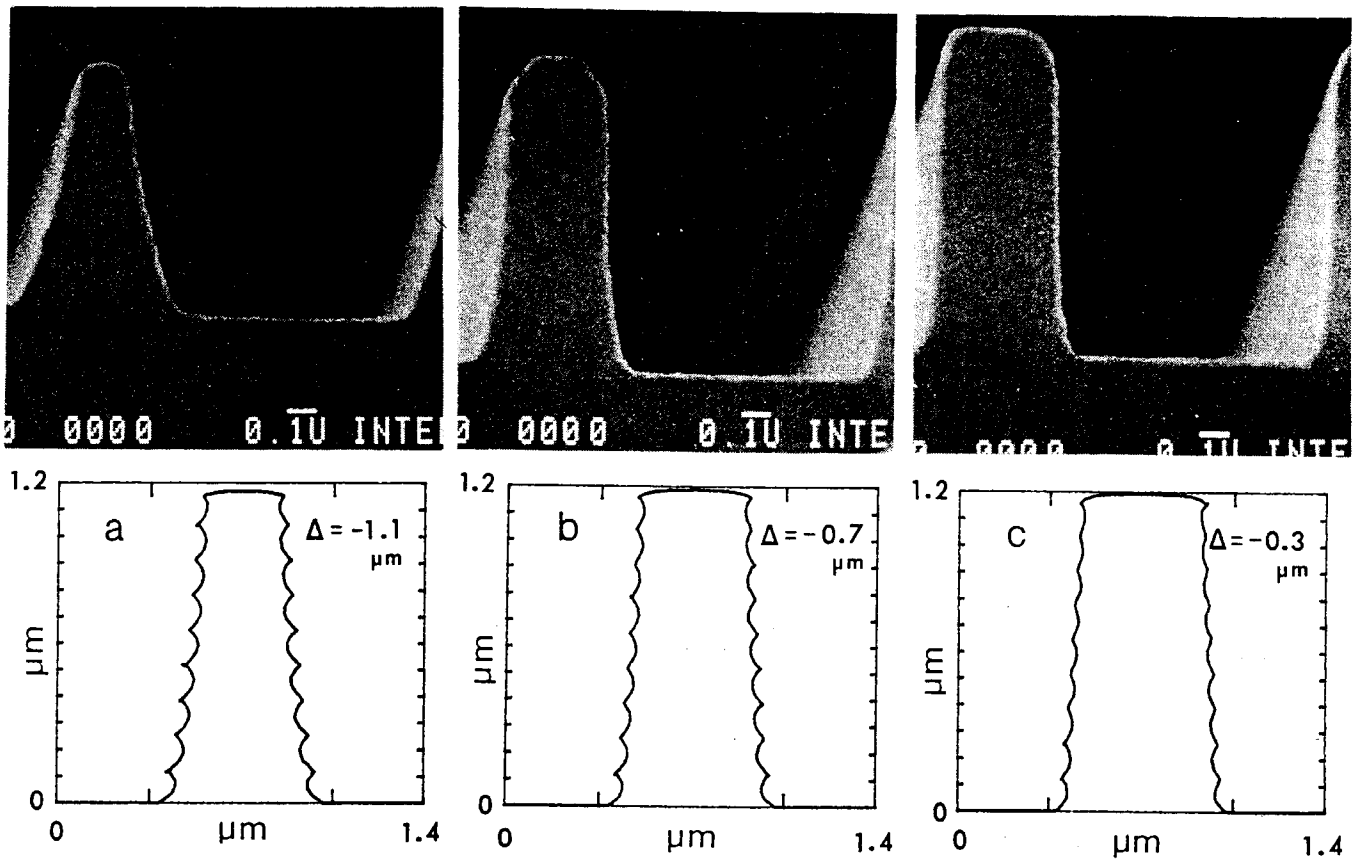

Figure 6. Experimental and simulated developed photoresist profiles for different values of focus but the same exposure dose. The object consisted of equal lines and spaces of width 0.70 µm. The optical system was a 5:1 reduction system with NA = 0.45, λ = 0.4358 µm and condenser NA to lens NA ratio = 0.5. The exposure dose

(continued next page)

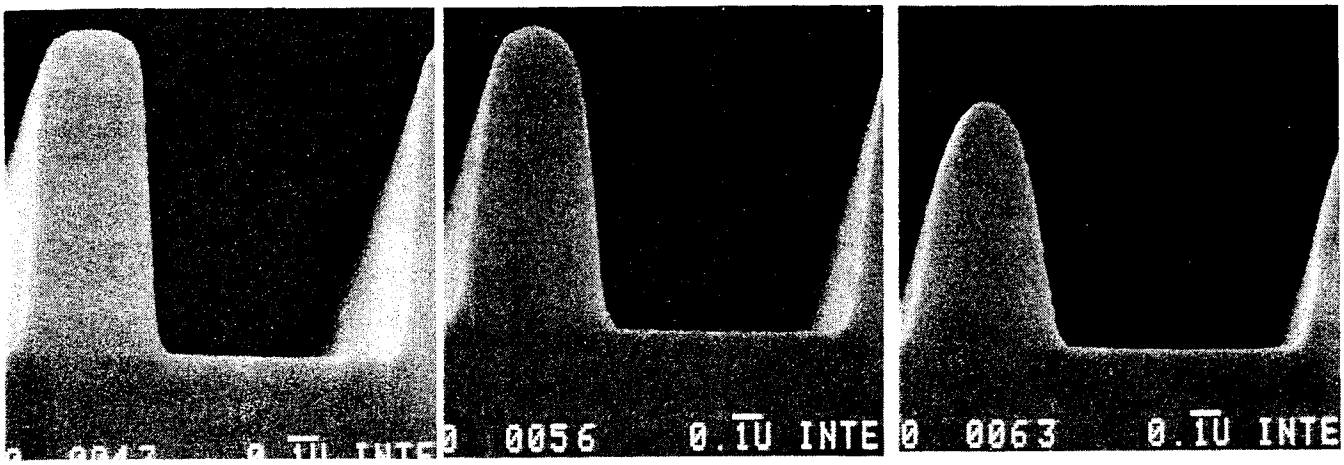

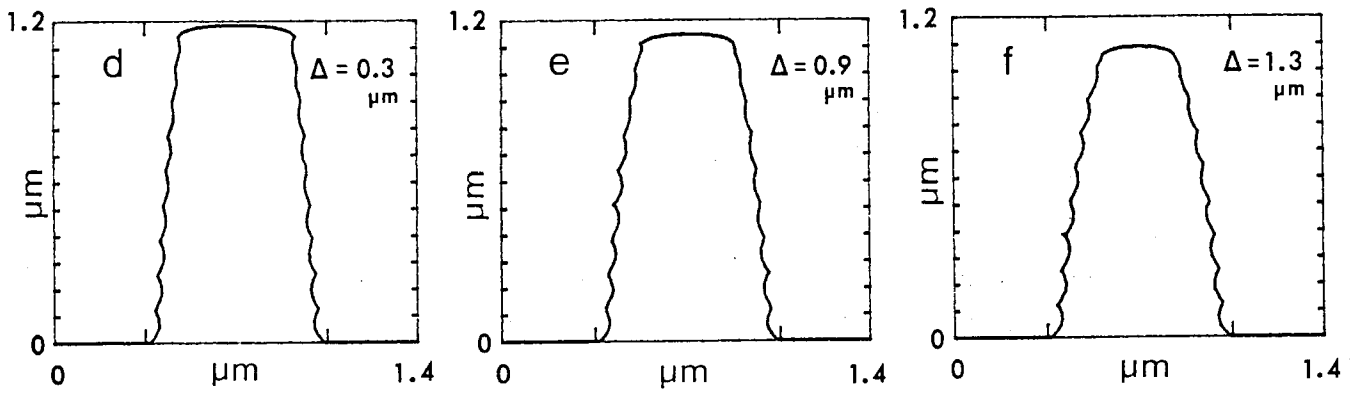

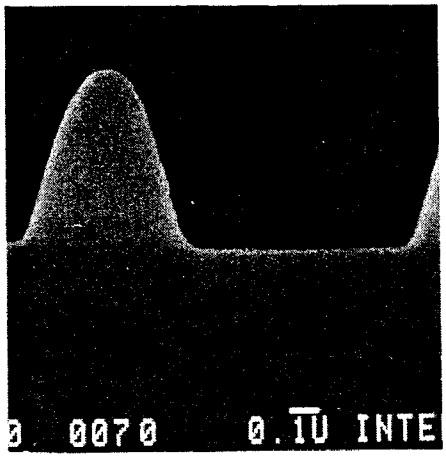

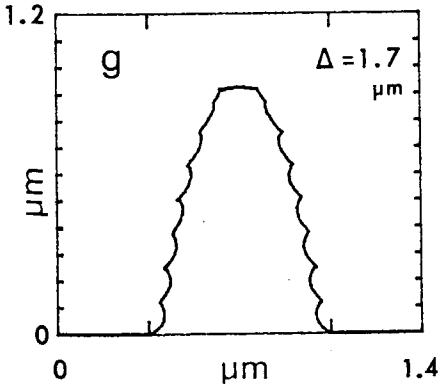

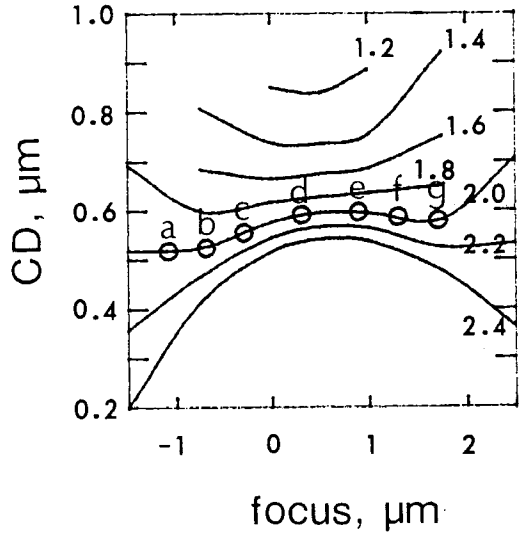

Insert showing the points in the calculated CD versus focus plot corresponding to the simulated profiles (a) to (g). To obtain the best agreement with experiment, the sequence of simulated profiles was shifted in focus compared to the SEM sequence by 1.3 μm, that is, experimental focus = Δ - 1.3 μm.

Figure 6. (continued:) was 2.0 times the threshold dose in all cases (see the caption of Fig. 2 for the meaning of threshold dose). The photoresist (TSMR8800) thickness was 1.20 μm and the substrate was silicon. The modeling parameters given in Table 1 for the AZ resists were used for the TSMR resist also.